THREE-BODY FORCES: FROM COLD ATOMS TO NUCLEI*

H.-W. Hammer

Institut für Kernphysik, Technische Universität Darmstadt
64289 Darmstadt, Germany
and
ExtreMe Matter Institute EMMI, GSI Helmholtzzentrum für
Schwerionenforschung GmbH, 64291 Darmstadt, Germany

(Received January 29, 2015)

Three- and higher-body forces enter naturally in effective field theories for strongly interacting quantum systems. We focus on the effect of three-body forces in systems close to the unitary limit and discuss applications in ultracold atoms and halo nuclei.

DOI:10.5506/APhysPolB.46.379
PACS numbers: 21.45.–v, 21.10.–k, 67.85.–d

1. Preliminary remarks

Three-body forces play an important role in quantum systems. Even if they are not present at a fundamental level, three- and higher-body forces appear in effective theories or in practical calculations, where the degrees of freedom and the Hilbert space have to be restricted.

In this paper, we approach the issue of three-body forces from an effective field theory (EFT) perspective (see Ref. [1] for a recent review following this philosophy). The concept of *resolution* plays a key role in this context. A particle beam with de Broglie wavelength λ can only probe structures at a scale $R \gtrsim \lambda$. Similarly, in a general process with typical momentum scale μ only physics at momenta $p \lesssim \mu$ (or, equivalently, distances $R \gtrsim 1/\mu$) is resolved. Effective theories and the renormalization group provide a method to exploit this observation for quantitative calculations. The resolution scale in an effective theory is controlled by the momentum cutoff Λ. Physics at momentum scales larger than the cutoff is excluded from the effective theory and encoded in effective couplings, so-called low-energy constants.

* Presented at the Zakopane Conference on Nuclear Physics "Extremes of the Nuclear Landscape", Zakopane, Poland, August 31–September 7, 2014.

These constants and the relative size of two- and higher-body forces turn out to be resolution dependent. If one starts with two-body forces only at high resolution, many-body forces will appear naturally as the resolution scale is lowered. These induced many-body forces capture the contributions of successive two-body interactions which are separated by a distance below the resolution scale.

As discussed above, the interaction strength may be shifted from two- to many-body forces by changing the momentum cutoff Λ in the regulators used in explicit calculations. Once the couplings of the effective Lagrangian, the low-energy constants (LECs), have been adjusted to selected data, predictions for other low-energy observables are independent of the choice for Λ. Thus, the interaction strengths of two- and many-body interactions vary with the cutoff and are not unique. The idea is illustrated in Fig. 1, where iterated two-body interactions at short-distance scales $|x - y| \sim 1/\Lambda$ are not resolved. Note that in practice the 3-body forces generated in this way cannot be disentangled from the 3-body forces at an initial scale, which will also have short-ranged (and other) contributions. It is, therefore, model-dependent to distinguish such "generated" from "genuine" 3-body forces.

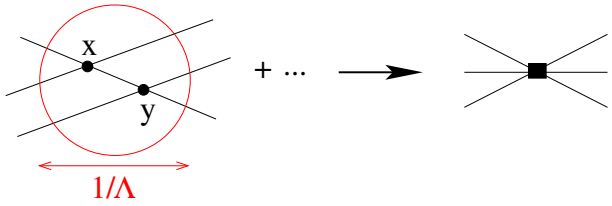

Fig. 1. Illustration for the resolution dependence of two- and three-body interactions.

2. Physics near the unitary limit

As discussed in the previous section, the short-distance properties of a physical system are not resolved in low-energy observables. If no massless particles are present, all interactions appear short-ranged at sufficiently low energy and one can use an EFT with contact interactions.

Here, we focus on systems close to the unitary limit of infinite scattering length. This hypothetical limit is obtained by taking the range of the interaction to zero while keeping a two-body bound state fixed at zero energy. The two-body scattering amplitude is then scale invariant and saturates the unitarity bound. Ultracold atomic gases can be tuned to the vicinity of the unitary limit using Feshbach resonances, while neutron matter is close to

this limit through a fine tuning in nature. This gives rise to novel many-body phenomena, such as the BEC-BCS crossover in ultracold atoms [2] and the "perfect" liquid observed in heavy-ion collisions [3].

Here, we use the unitary limit as a starting point for an EFT expansion for strongly-interacting quantum systems with short-range interactions. This universal EFT is applicable to any system close to the unitary limit, *i.e.*, any system with short range interactions and large scattering lengths. Examples include halo states in nuclear physics, ultracold atoms close to a Feshbach resonance, and hadronic molecules in particle physics. The breakdown scale $M_{\rm high}$ of this theory is set by the lowest energy degree-of-freedom not explicitly included in the theory. In nuclear and particle physics, this is typically given by one-pion exchange. In ultracold atoms, $M_{\rm high}$ is determined by the van der Waals interaction, but the details depend on the system. The typical momentum scale of the theory is $M_{\rm low} \sim 1/a \sim k$. For momenta k of the order of the breakdown scale $M_{\rm high}$ or above, the omitted short-range physics is resolved and has to be treated explicitly.

The universal EFT exploits the appearance of a large scattering length, independent of the mechanism generating it. Because the dependence of observables on the scattering length is explicit, it allows to unravel universal phenomena driven by the large scattering length such as universal correlations of observables, the Efimov effect [4], and limit cycle physics [5]. For reviews of applications to the physics of ultracold atoms, nuclear, and particle physics see, *e.g.*, Refs. [6–8].

Three-body forces play an important role in the universal EFT and we discuss their contribution in three- and higher-body systems in detail below. In the simplest case of spinless bosons, the leading order Lagrangian can be written as

$$\mathcal{L} = \psi^\dagger \left(i\partial_t + \frac{\vec{\nabla}^2}{2m} \right) \psi - g_2 \left(\psi^\dagger \psi \right)^2 - g_3 \left(\psi^\dagger \psi \right)^3 + \dots \,. \tag{1}$$

Extensions to more complicated systems are straightforward. The terms proportional to g_2 and g_3 correspond to two- and three-body contact interactions. The dots represent higher-order terms suppressed by derivatives and/or more fields.

The renormalized values of the coupling constants g_2 and g_3 are matched to observables in the two- and three-body system. In the two-body system, one typically takes the S-wave scattering length. The exact relation between the coupling g_2 and the scattering length depends on the renormalization scheme. Because of this matching procedure, the EFT provides correlations between different observables based on the hierarchy of scales in the system.

Given one set of observables, another set can be predicted to a certain accuracy. Depending on the experimental situation, these correlations can be applied in different ways.

Since the scattering length is large, $a \sim 1/M_{\rm low}$, the leading contact interaction g_2 has to be resummed to all orders [9, 10]. The two-body scattering amplitude is obtained by summing the bubble diagrams with the g_2 interaction shown in Fig. 2. This summation gives the exact solution of the Lippmann–Schwinger equation for the g_2 interaction and reproduces the leading term of the effective range expansion, $T_2(k) = (4\pi/m)\,[-1/a - ik]^{-1}$. Higher-order derivative interactions, which are not shown explicitly in Eq. (1), generate higher-order terms in the effective range expansion. Since these terms are set by $M_{\rm high}$, their contribution at low energies is suppressed by powers of $M_{\rm low}/M_{\rm high}$ and can be treated in perturbation theory. The first correction is given by the S-wave effective range, $r_0 \sim 1/M_{\rm high}$.

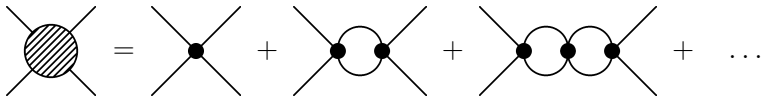

Fig. 2. The bubble diagrams with the contact interaction g_2 contributing to the two-body scattering amplitude.

The universal EFT shows its full strength in the two-body sector when external currents are considered. In contrast to other approaches, the coupling to currents is straightforward and current conservation is satisfied at each stage of the calculation. Gauge invariant few-body contact terms are generated naturally by writing the most general effective Lagrangian.

We now proceed to the three-body system where the term proportional to g_3 in Eq. (1) contributes. From naive dimensional analysis, one would conclude that the g_3 term is of higher order. This is, indeed, the case for two-component fermions where the Pauli principle forbids three fermions to be close together in an S-wave. In general, however, naive dimensional analysis fails for large scattering length a. Again, we focus on the case of identical bosons which already contains the main features of the problem. The simplest three-body process to be considered is the scattering of a boson and a dimer. The integral equation for boson-dimer scattering is shown schematically in Fig. 3. For total orbital angular momentum $L = 0$, it takes the form

$$T_3(k,p;\,E) \;=\; \frac{16}{3a}\,M(k,p;\,E) + \frac{4}{\pi}\int\limits_0^\Lambda dq\,\frac{q^2\,T_3(k,q;\,E)\,M(q,p;\,E)}{-\frac{1}{a}+\sqrt{3q^2/4 - mE - i\epsilon}}\,, \quad (2)$$

where the inhomogeneous term reads

$$M(k,p;\,E) = \frac{1}{2kp}\ln\left(\frac{k^2+kp+p^2-mE}{k^2-kp+p^2-mE}\right) + \frac{H(\Lambda)}{\Lambda^2}\,, \tag{3}$$

and a momentum cutoff Λ has been introduced to regulate the integral equation. All other three-body observables can be extracted from the amplitude T_3 taken in appropriate kinematics. In Eq. (2), H determines the strength of the three-body interaction $g_3(\Lambda) = -4m\,g_2(\Lambda)^2 H(\Lambda)/\Lambda^2$. The magnitude of the incoming (outgoing) relative momenta is k (p) and $E = 3k^2/(4m) - 1/(ma^2)$. The on-shell point corresponds to $k = p$ and the scattering phase shift can be obtained via $k\cot\delta = 1/T_3(k,k;\,E) + ik$.

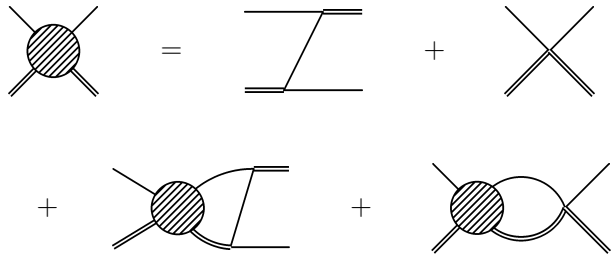

Fig. 3. The integral equation for the boson-dimer scattering amplitude. The single (double) line indicates the boson (dimer) propagator.

For $H = 0$ and $\Lambda \to \infty$, Eq. (2) reduces to the Skorniakov–Ter–Martirosian equation [11] which has no unique solution. The regularized equation has a unique solution for any given (finite) value of the cutoff Λ but three-body observables show a strong dependence on the cutoff Λ. Cutoff independence of the amplitude is restored by an appropriate "running" of $H(\Lambda)$ which turns out to be a limit cycle [12]

$$H(\Lambda) \approx \frac{\cos\left[s_0\ln\left(\Lambda/\Lambda_*\right) + \arctan s_0\right]}{\cos\left[s_0\ln\left(\Lambda/\Lambda_*\right) - \arctan s_0\right]}\,, \tag{4}$$

where $s_0 \approx 1.00624$ is a transcendental number and Λ_* is a dimensionful three-body parameter generated by dimensional transmutation. Adjusting Λ_* to a single three-body observable allows to determine all other low-energy properties of the three-body system. Note that the choice of the three-body parameter Λ_* is not unique and there are other definitions more directly related to experiment [6].

The physics of this renormalization procedure is illustrated in Fig. 4 where we show the unrenormalized three-body binding energies B_3 in the case of positive scattering length as a function of the cutoff Λ (solid line).

As the cutoff is increased, B_3 increases. At a certain cutoff (indicated by the dotted line), a new bound state appears at the boson-dimer threshold. This pattern repeats every time the cutoff increases by the discrete scaling factor $\exp(\pi/s_0)$. Now assume that we adopt the renormalization condition that the shallowest state should have a constant energy given by the dashed line. At small values of the cutoff, we need an attractive three-body force to increase the binding energy of the shallowest state as indicated by the arrow. As the cutoff is increased further, the required attractive contribution becomes smaller and around $\Lambda a = 1.1$ a repulsive three-body force is required (downward arrow). Around $\Lambda a = 4.25$, a new three-body state appears at threshold and we cannot satisfy the renormalization condition by keeping the first state at the required energy any more. The number of bound states has changed and there is a new shallow state in the system. At this point, the three-body force turns from repulsive to attractive to move the new state to the required energy. The corresponding running of the three-body force with the cutoff Λ is shown in the inset. After renormalization, the first state is still present as a deep state with large binding energy, but for threshold physics its presence can be ignored. This pattern goes on further and further as the cutoff is increased. The extension to systems with more three-body states is straightforward.

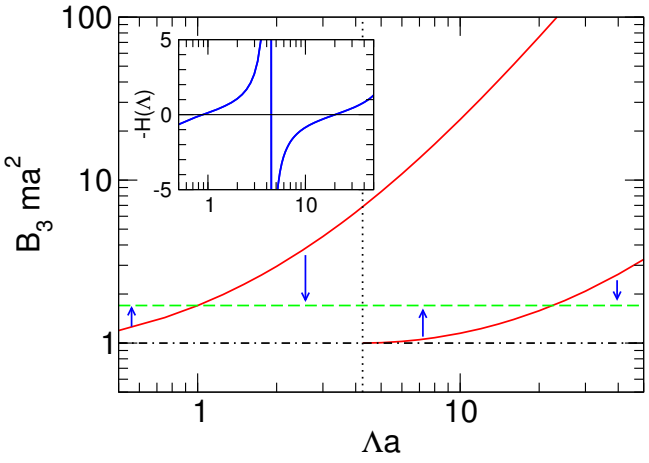

Fig. 4. Unrenormalized three-body energies B_3 as a function of the momentum cutoff Λ (solid lines). The dotted line indicates the cutoff where a new three-body state appears at the boson-dimer threshold (dash-dotted line). The dashed line shows a hypothetical renormalized energy. The inset shows the running of the three-body force $g_3(\Lambda) \sim -H(\Lambda)$ with Λ.

The three-body force in Eq. (4) has exactly the right behavior to implement the strategy from the previous paragraph. Moreover, it breaks the scale invariance in the unitary limit since the three-body parameter Λ_* now provides a scale. However, due to the specific form of Eq. (4), a discrete scale invariance survives. Scaling transformations with the scaling factor $\lambda_0 = \exp(\pi/s_0)$ leave $H(\Lambda)$ and, consequently, three-body observables invariant. This discrete scaling symmetry is the signature of an RG limit cycle [13]. In the three-body bound-state spectrum, it becomes manifest through the *Efimov effect*: The appearance of a geometric spectrum of three-body bound states [4].

The Efimov spectrum is illustrated in the left panel of Fig. 5. We show the energy variable $K = \mathrm{sgn}(E)\sqrt{m|E|}$ as a function of the inverse scattering length $1/a$. The hashed areas indicate the three-atom ($a < 0$) and atom-dimer thresholds ($a > 0$) where the Efimov states become unstable. The spectrum is invariant under the discrete scaling transformations $K \to \lambda_0 K$ and $1/a \to \lambda_0/a$. As a consequence, there is an accumulation of Efimov three-body states at the origin. The scaling symmetry relates Efimov states along any ray with fixed angle ξ (*cf.* Fig. 5). In general, these states correspond to different scattering lengths. A physical system with fixed scattering length is illustrated by the vertical dashed line. For fixed a, the discrete scaling symmetry is only manifest in the unitary limit $1/a = 0$.

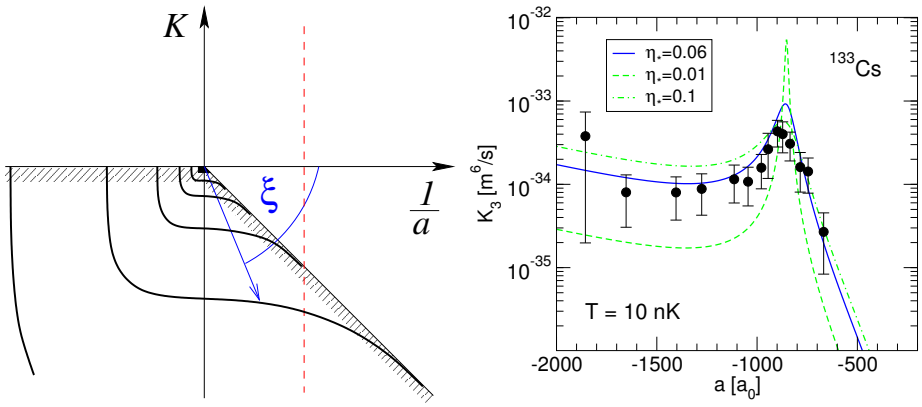

Fig. 5. Left panel: Illustration of the Efimov spectrum: The energy variable $K = \mathrm{sgn}(E)\sqrt{m|E|}$ is shown as a function of the inverse scattering length $1/a$. The solid lines indicate the Efimov states, while the hashed areas give the scattering thresholds. The dashed vertical line indicates a system with fixed scattering length. Right panel: The 3-body loss coefficient K_3 in ^{133}Cs for negative values of the scattering length near the Efimov resonance at $a \approx 850 a_0$. The data points are for $T = 10$ nK and are taken from Ref. [17].

The parameter Λ_* can be used to set one of the three-body energies. All other states then follow from the discrete scaling symmetry. This explains why one parameter is sufficient for renormalization of the whole spectrum. The discrete scaling symmetry predicts infinitely-deep three-body states. This is known as the Thomas collapse [14]. Physically relevant, however, are only states with energies $|E| \ll M_{\rm high}^2/m$. All deeper states are ultraviolet artefacts of the effective theory and should be discarded.

3. Ultracold atoms

The discrete scale invariance also manifests itself in the log-periodic dependence of scattering observables on the scattering length. This scaling behavior has been confirmed in cold atom experiments [15]. In such experiments, the scattering length can be varied using Feshbach resonances. The scattering-length dependence of three-body recombination rates provides indirect information on the Efimov spectrum. For negative scattering length, the Efimov states hit the three-atom threshold, $E = 0$, for certain values of a (*cf.* Fig. 5) and lead to enhanced recombination rates. For positive scattering length, the Efimov states become unstable already at the atom-dimer threshold, $E = -1/(ma^2)$, but interference effects lead to minima and maxima in the rate at $E = 0$. Ideally, one would like to see multiple recombination features on each side of the resonance at $1/a = 0$. For equal mass particles, this is not a simple task because of the large scaling factor. When effective range effects are included perturbatively, the discrete scale invariance is softly broken but the effects of the breaking on the recombination rate can be calculated [16].

As an example, we show the three-body loss coefficient K_3 in a gas of ultracold ^{133}Li atoms measured by the Grimm group [17] as a function of scattering length in the right panel of Fig. 5. This was the first experiment to provide evidence for Efimov states in ultracold gases. The line shape of the loss resonance is well described by the prediction from the universal EFT [6]. The current challenges in the field of ultracold atoms include the detection of excited Efimov trimers. Here, mixtures of atoms with different masses are interesting since they can have a smaller scaling factor. A recent highlight includes the observation of ground and excited state trimers in a Li–Cs mixture [18, 19].

4. Halo nuclei

Two-neutron halo nuclei provide another arena for observing physics of the unitary limit and the Efimov effect. Since the strength of the interaction between the neutrons and the core is fixed, however, the scattering

length dependence of observables cannot be used to identify Efimov physics. Instead, one can look for excited states which (approximately) satisfy the universal scaling relation for bound states. Several nuclear systems have been discussed as possible candidates for Efimov states. The current status according to a recent EFT analysis of a number of established halo nuclei [20] which did not indicate any excited states is summarized in Fig. 6.

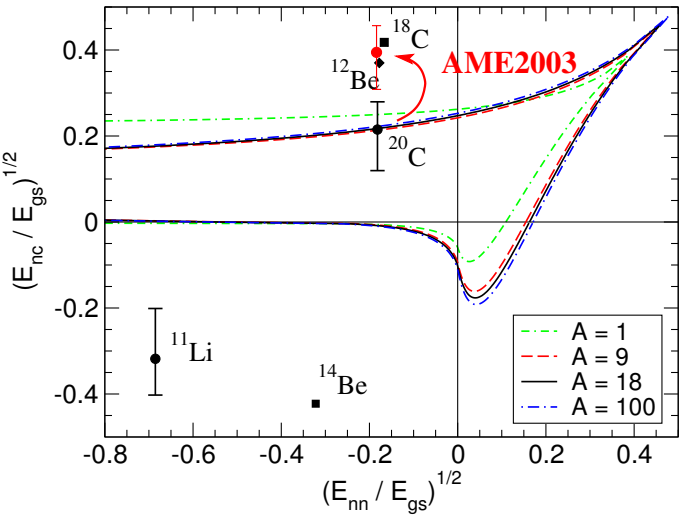

Fig. 6. Boundary curves for the existence of an excited Efimov state as function of the neutron–core energy E_{nc} and neutron–neutron energy E_{nn} in units of the three-body ground state energy $E_{\rm gs}$. The shift of ^{20}C from using the values of the newer AME2003 atomic mass evaluation [21] is indicated by the arrow.

The most promising system known so far is the ^{22}C halo nucleus which was found to display an extremely large matter radius [22] and is known to have a significant S-wave component in the n–^{20}C system [23]. Acharya *et al.* [24], however, also excluded an excited Efimov state in ^{22}C.

Whether heavier two-neutron halos exist is still an open question. There has been much interest, both experimental and theoretical, in determining precise values for masses, understanding shell evolution and the location of the dripline in the neutron-rich calcium isotopes [25–28]. Coupled-cluster calculations of neutron-rich calcium isotopes that included coupling to the scattering continuum and schematic three-nucleon forces, suggested that there is an inversion of the *gds* shell-model orbitals in ^{53,55,61}Ca. In particular, it was suggested that a large S-wave scattering length might occur in ^{61}Ca with interesting implications for ^{62}Ca.

Hagen *et al.* [29] used the coupled-cluster method combined with modern chiral effective theory interactions and follow the method outlined in Ref. [30] to compute the elastic scattering of neutrons on ^{60}Ca. They analyzed the resulting phase-shift data to obtain quantitative estimates for the scattering length and the effective range and showed that a large scattering length can be expected in this system. The results obtained from *ab inito* calculations were then used as input for the so-called halo effective field theory (EFT) that describes the halo system in terms of its effective degrees of freedom (core and valence nucleons) [31, 32]. They used halo EFT to analyze the implications of the coupled cluster results for the ^{60}Ca–n–n system. Specifically, they focused on the signals of Efimov physics that are a consequence of the large scattering length in the ^{60}Ca–n and n–n systems.

For ^{62}Ca, the discrete scaling factor governing the energy spectrum is approximately $16^2 = 256$. The exact scaling symmetry applies for deep states and in the unitary limit of infinite scattering length. For two levels near threshold, however, the ratio of their energies can be significantly smaller if one of the states is very close to the threshold. In the ^{62}Ca case, the whole energy region between $S_n \approx 5$–8 keV and the breakdown scale $S_{\rm deep} \approx 500$ keV is available for Efimov states in ^{62}Ca. It is thus conceivable that ^{62}Ca would display an excited Efimov state and unlikely that it would not display any Efimov states.

The results of Hagen *et al.* [29] imply that ^{62}Ca is possibly the largest and heaviest halo nucleus in the chart of nuclei. They showed that, as a result, a large number of observables would display characteristic features that could be used to test our hypothesis. Measurements of these observables will clearly pose a significant challenge for experiment. For example, ^{58}Ca is the heaviest calcium isotope that has been observed experimentally [33]. However, future RIB facilities might provide access to calcium isotopes as heavy as ^{68}Ca and thereby facilitate a test of this hypothesis.

5. Conclusion

In this contribution, we have highlighted the importance of three-body forces in the universal EFT which is based on an expansion around the unitary limit. Here, three-body forces contribute already at leading order because of the Efimov effect. We discussed several application in nuclear physics and ultracold atoms in detail.

In the chiral EFT, which is valid for typical momenta up to the order a few times the pion mass, three-body forces are suppressed compared to two-body interactions and enter only at next-to-next-to-leading order. Nevertheless, for applications of chiral EFT interactions to nuclear structure, three-body forces have been shown to play a central role for light and

medium-mass nuclei as well as nuclear matter. We did not have the space to cover these important developments in this paper, but an excellent overview of the status and challenges of three-body forces in nuclear structure and beyond can be found in Ref. [1].

This work was supported by the DFG through funds provided to the Sino-German CRC 110, by the BMBF under contract 05P12PDFTE, and by the Helmholtz Association under contract HA216/EMMI.

REFERENCES

[1] H.-W. Hammer, A. Nogga, A. Schwenk, *Rev. Mod. Phys.* **85**, 197 (2013).
[2] S. Giorgini, L.P. Pitaevskii, S. Stringari, *Rev. Mod. Phys.* **80**, 1215 (2008).
[3] T. Schäfer, D. Teaney, *Rep. Prog. Phys.* **72**, 126001 (2009).
[4] V. Efimov, *Phys. Lett.* **B33**, 563 (1970).
[5] E. Braaten, H.-W. Hammer, *Phys. Rev. Lett.* **91**, 102002 (2003).
[6] E. Braaten, H.-W. Hammer, *Phys. Rep.* **428**, 259 (2006).
[7] E. Epelbaum, H.-W. Hammer, U.-G. Meißner, *Rev. Mod. Phys.* **81**, 1773 (2009).
[8] H.-W. Hammer, L. Platter, *Annu. Rev. Nucl. Part. Sci.* **60**, 207 (2010).
[9] D.B. Kaplan, M.J. Savage, M.B. Wise, *Nucl. Phys.* **B534**, 329 (1998).
[10] U. van Kolck, *Nucl. Phys.* **A645**, 273 (1999).
[11] G.V. Skorniakov, K.A. Ter-Martirosian, *Sov. Phys. JETP* **4**, 648 (1957).
[12] P.F. Bedaque, H.-W. Hammer, U. van Kolck, *Phys. Rev. Lett.* **82**, 463 (1999).
[13] K.G. Wilson, *Phys. Rev.* **D3**, 1818 (1971).
[14] L.H. Thomas, *Phys. Rev.* **47**, 903 (1935).
[15] F. Ferlaino, R. Grimm, *Physics* **3**, 9 (2010).
[16] C. Ji, D.R. Phillips, L. Platter, *Ann. Phys.* **327**, 1803 (2012).
[17] T. Kraemer *et al.*, *Nature* **440**, 315 (2006).
[18] R. Pires *et al.*, *Phys. Rev. Lett.* **112**, 250404 (2014).
[19] S.K. Tung *et al.*, *Phys. Rev. Lett.* **113**, 240402 (2014).
[20] D.L. Canham, H.-W. Hammer, *Eur. Phys. J.* **A37**, 367 (2008).
[21] G. Audi, A.H. Wapstra, C. Thibault, *Nucl. Phys.* **A729**, 337 (2003).
[22] K. Tanaka *et al.*, *Phys. Rev. Lett.* **104**, 062701 (2010).
[23] W. Horiuchi, Y. Suzuki, *Phys. Rev.* **C74**, 034311 (2006).
[24] B. Acharya, C. Ji, D.R. Phillips, *Phys. Lett.* **B723**, 196 (2013).
[25] A. Lapierre *et al.*, *Phys. Rev.* **C85**, 024317 (2012); A.T. Gallant *et al.*, *Phys. Rev. Lett.* **109**, 032506 (2012).

[26] J.D. Holt, A. Schwenk, *J. Phys. G* **39**, 085111 (2012).
[27] G. Hagen *et al.*, *Phys. Rev. Lett.* **109**, 032502 (2012).
[28] W. Nazarewicz *et al.*, *Phys. Rev.* **C53**, 740 (1996); J. Erler *et al.*, *Nature* **486**, 509 (2012).
[29] G. Hagen, P. Hagen, H.-W. Hammer, L. Platter, *Phys. Rev. Lett.* **111**, 132501 (2013).
[30] G. Hagen, N. Michel, *Phys. Rev.* **C86**, 021602(R) (2012).
[31] C.A. Bertulani, H.-W. Hammer, U. van Kolck, *Nucl. Phys.* **A712**, 37 (2002).
[32] P.F. Bedaque, H.-W. Hammer, U. van Kolck, *Phys. Lett.* **B569**, 159 (2003).
[33] O.B. Tarasov *et al.*, *Phys. Rev. Lett.* **102**, 142501 (2009).